frontiers | Frontiers in Earth Science

TYPE Original Research
PUBLISHED 18 January 2023
DOI 10.3389/feart.2022.1057831

OPEN ACCESS

EDITED BY
Mingjun Zou,
North China University of Water Resources and Electric Power, China

REVIEWED BY
Haihai Hou,
Liaoning Technical University, China
Jun Shen,
China University of Geosciences Wuhan, China
Dongdong Wang,
Shandong University of Science and Technology, China

*CORRESPONDENCE
Juan Wang,
66676872@qq.com

SPECIALTY SECTION
This article was submitted to Economic Geology, a section of the journal Frontiers in Earth Science

RECEIVED 30 September 2022
ACCEPTED 31 October 2022
PUBLISHED 18 January 2023

CITATION
Wang J, Shao L, Yan Z and Wang X (2023), The coal-forming environment during mass extinction in the latest permian: Evidence from geochemistry of rare Earth elements.
Front. Earth Sci. 10:1057831.
doi: 10.3389/feart.2022.1057831

The coal-forming environment during mass extinction in the latest permian: Evidence from geochemistry of rare Earth elements

Juan Wang[1,2,3]*, Longyi Shao[2], Zhiming Yan[2] and Xuetian Wang[2]

[1]School of Resources and Environment, Henan Polytechnic University, Jiaozuo, China, [2]State Key Laboratory of Coal Resources and Safe Mining, College of Geoscience and Surveying Engineering, China University of Mining and Technology (Beijing), Beijing, China, [3]Collaborative Innovation Center of Coal Work Safety and Clean High Efficiency Utilization, Jiaozuo, China

The C_1 coal of Latest Permian during mass extinction in eastern Yunnan was studied to reveal the terrestrial paleoenvironment and influence of geological events on coal-formation during mass extinction. An analysis of Rare Earth Elements (REEs) was conducted on the C_1 coal from the Yantang Mine of Xuanwei, eastern Yunnan Province, which was deposited during the latest Permian. A total of 24 samples from coals, partings, roofs and floors from the C_1 coal were taken from the fresh face in the underground mine. The results of the REEs analysis indicated that the total REE content (∑REE) in the C_1 coal varies from 23.99 μg/g to 267.94 μg/g, averaged 122.69 μg/g. The C_1 coal is enriched in light REE (LREE) relative to heavy REE (HREE), signifying the fractionation between LREE and HREE. Most samples of the coal seam C_1 are depleted in Eu in various degrees and slightly depleted in Ce, especially two partings in sub-seams B_1 and B_3 which show the significant negative Eu anomalies. The geochemical characteristics of REE reveal that the C_1 coal was deposited in a weak oxidation environment; the sedimentary environment was turbulent during the middle-later stage of coal-forming process; the C_1 coal was affected by the basalt clastic materials from the Khangdian Oldland and acidic synsedimentary volcanic ash in the coal-forming period. The geochemical characteristics of Tonsteins in C_1 coal are similar to those of marine Permian-Triassic boundary (PTB) volcanic ash layers in South China, which are both derived from the felsic volcanism caused by the closure of the Paleo-Tethys at the southwestern margin of the South China. Furthermore, the C_1 coal was also affected by the eruption of Siberian large igneous province (SLIP) in the early stage.

KEYWORDS

the latest Permian, rare Earth elements, coal-forming environment, volcanism, eastern Yunnan

1 Introduction

Rare Earth elements (REEs) present relatively stable chemical properties as well as a high degree of uniformity, and are easily preserved in a geologic body after sedimentation. The information about the sediment provenance that REEs carry is not easy to lose and is little affected by metamorphism. Therefore, REEs have been used as powerful geochemical indicators to reflect provenance compositions and changes, and provide geochemical evidences for the formation and evolution of coal seams (Wang et al., 2008; Xie et al., 2014; Arbuzov et al., 2018). At present, many studies on REEs in coals have been focusing on the characteristics of contents and the spatial distribution, occurrence, distribution pattern, provenance analysis and primary sedimentary environment of coals (Hao et al., 2004; Ren et al., 2006; Wu et al., 2013; Liu et al., 2015; Munir et al., 2018; Hedin et al., 2019; Ulrich et al., 2019). However, fewer studies have focused on the relationships between the geochemical characteristics of REEs and special geological events.

End-Permian time is one of the most important critical transition in geological history, and the largest mass extinction occurred at the Permian-Triassic transition (Wang et al., 2018; Guo et al., 2022). As the last coal deposited at the end Permian, the C_1 coal recorded the terrestrial paleoenvironment changes during mass extinction (Wang et al., 2018), the geochemical characteristics of C_1 coal may be closely related to the event. The geochemical characteristics of trace elements other than REEs have been studied by Shao et al. (2015), and they proposed that enriched elements mainly derived from continental weathering of the Emeishan basalt, synsedimentary volcanic ashes and medium-low temperature hydrothermal fluid. REEs, however, are more reliable tracers to reveal provenance and paleoenvironment, and can better constrain the environment and biological evolution events (Tian et al., 2014). In this paper, systematic REEs geochemical analyses of the latest Permian C_1 coal in Xuanwei county have been conducted, combined with previous research results about major and trace elements in C_1 coal to accurately trace the provenance change during the coal forming (Shao et al., 2015), reveal the sedimentary environment and tectonic background of coal forming, and discuss a series of geological events occurred on land during the mass extinction at the latest Permian, especially the effects of volcanic activities on coal-formation.

2 Geological setting

Xuanwei County is located in the eastern Yunnan Province and adjacent to the west Guizhou Province (Figure 1), which was tectonically located in the western part of the South China cratonic basin during the Late Permian (Shao et al., 2013). The siliciclastic sediments in this area were supplied predominantly by the Khangdian Oldland to the west. Meanwhile a long-term gradual easterly transgression throughout Late Permian provided sufficient accommodation space for the development of this important latest Permian coal province (Wang et al., 2011; Shao et al., 2013). The C_1 coal is widely distributed in eastern Yunnan, mainly located in

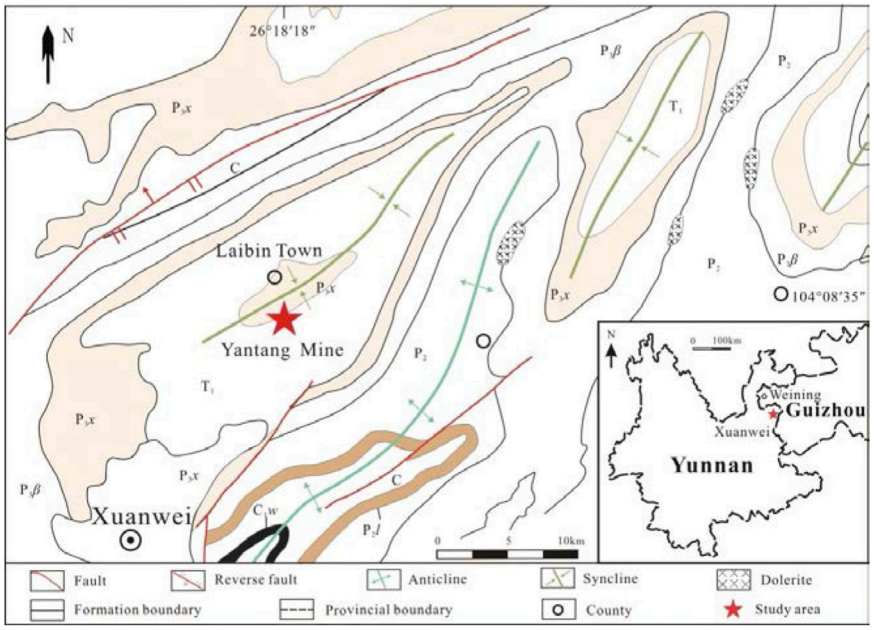

FIGURE 1
Location of the Yantang mine, Laibin Town, Xuanwei county, Yunnan Province (cited from Wang et al., 2018).

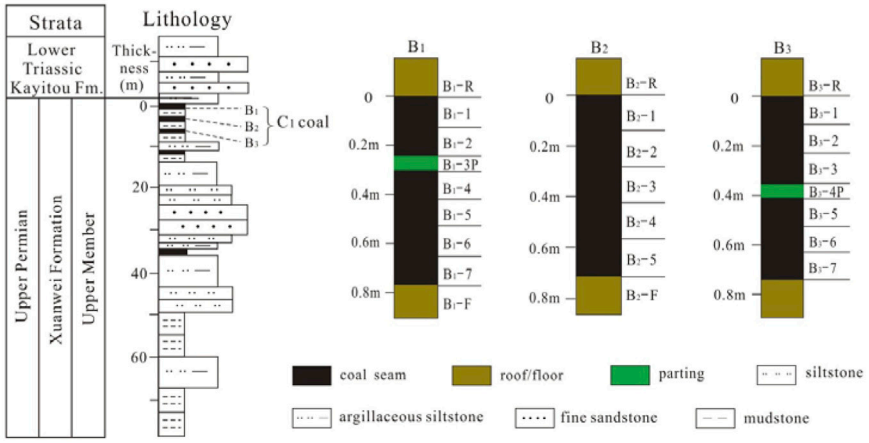

FIGURE 2
The stratigraphic section of mineable coal seam and sampling horizons of the Yantang Mine.

Xuanwei, Fuyuan and Weining areas, and lied in the uppermost portion of the Xuanwei Formation of Late Permian. The Xuanwei Formation unconformably underlaid by the Emeishan Basalt, and is conformably overlaid by the Kayitou Formation of Early Triassic (Figure 2). In the Xuanwei area, this formation consists mainly of grey fine-grained sandstone, siltstone and mudstone, some volcanic ash beds, and numerous coal seams including the C_1 coal seam at its top (Wang et al., 2012). The Xuanwei Formation of Late Permian is mostly made of continental fluvial deposits (Wang et al., 2011).

TABLE 1 Partial proximate analysis, sulfur contents and vitrinite reflectance in coals from the Yantang Mine in Xuanwei, Yunnan (%).

No.	M_{ad}	A_d	V_d	$S_{t,d}$	$S_{s,d}$	$S_{p,d}$	$S_{o,d}$	R^o_{av}
B_1-1	1.86	63.36	12.13	0.24	0.03	0.18	0.03	1.28
B_1-2	0.90	48.21	14.15	0.12	0.01	0.10	0.01	1.26
B_1-4	1.12	28.32	20.30	0.10	bdl	0.07	0.03	1.37
B_1-5	1.16	40.29	16.91	0.06	bdl	0.05	0.01	1.31
B_1-6	0.91	32.11	16.95	0.17	bdl	0.16	0.01	1.24
B_1-7	0.93	27.54	19.65	0.07	bdl	0.03	0.04	1.27
B_2-1	1.16	37.01	17.53	0.38	0.02	0.30	0.06	1.19
B_2-2	0.96	23.06	20.93	0.22	0.02	0.19	0.01	1.25
B_2-3	0.94	61.32	9.68	0.19	0.01	0.17	0.01	nd
B_2-4	0.80	32.10	19.62	0.64	0.02	0.34	0.28	1.27
B_2-5	0.81	25.37	20.71	0.13	0.01	0.12	bdl	1.33
B_3-1	0.78	40.23	16.24	0.10	bdl	0.06	0.04	nd
B_3-2	0.31	27.55	19.66	0.10	0.01	0.03	0.06	nd
B_3-3	0.88	45.71	17.71	0.11	0.01	0.02	0.08	nd
B_3-5	0.99	17.80	24.94	0.10	0.01	bdl	0.09	nd
B_3-6	0.41	16.88	26.30	0.11	0.02	0.01	0.08	nd
B_3-7	0.25	22.43	27.16	0.11	0.02	0.02	0.07	nd

M, moisture; A, ash yield; V, volatile content; ad, air dry basis; d, dry basis; St, total sulfur; Ss, sulfate sulfur; Sp, pyritic sulfur; So, organic sulfur; Roav, average vitrinite reflectance. All data in Table 1 comes from Shao et al., 2015.

3 Sampling and experimental methods

3.1 Sample description and basic data

Samples were collected from the Yantang Mine of Laibin Town, Xuanwei County, and the coal seam C_1 is the only minable seam in this mine which included three sub-seams B_1, B_2, and B_3 in descending order. Within the sub-seam B_1 and B_3, a 5 cm-thick Tonstein (kaolinite claystone altered from volcanic ash) layer exists (Figure 2). The total of 24 collected coal-seam channel samples including coal, Tonstein, roof and floor, were taken from the fresh face of the underground mine. The sampling site was located at N 26°18′18″ and E 104°08′35″ and the samples were collected with a vertical spacing of about 10 cm. All samples collected were at least 1 kg in weight and were immediately stored in plastic bags to ensure as little contamination as possible. The method of sample collection followed the Chinese National Standard for Collecting Channel Samples GB/T 482-2008.

The partial proximate analysis, sulfur contents and vitrinite reflectance of C_1 coal are presented in Table 1. The analytical data show that all samples are bituminous coal with a medium-high ash yield, ultralow total sulfur content and low-medium volatile content. According to coal ash classification (GB/T 15224.1–94), the coal samples B_1-1 and B_2-3 are classified as mixture of coal and mudstone since their ash yields exceeds 50%. Therefore, these are not included in the discussion of the C_1 coal in the present paper.

TABLE 2 REE contents of the late permian coal seam samples from the Yantang Mine, Xuanwei, Yunnan (μg/g).

No.	La	Ce	Pr	Nd	Sm	Eu	Gd	Tb	Dy	Ho	Er	Tm	Yb	Lu
B_1-R	68.80	126.00	15.50	61.50	8.46	2.00	7.77	1.60	10.10	2.01	6.09	1.02	5.62	0.75
B_1-1	26.20	48.70	5.32	20.20	2.49	0.52	1.99	0.53	3.42	0.77	2.27	0.60	2.28	0.30
B_1-2	29.70	62.70	7.67	29.50	5.96	0.95	5.02	0.76	3.95	0.75	1.94	0.33	1.96	0.30
B_1-3P	60.00	117.00	13.50	51.40	10.20	1.71	10.60	2.42	14.90	2.98	9.81	1.52	10.70	1.67
B_1-4	35.90	80.50	10.00	42.90	9.00	1.49	9.61	2.10	11.20	2.26	6.52	0.99	5.65	0.86
B_1-5	33.30	65.65	7.77	30.10	5.58	0.87	4.73	0.76	3.91	0.83	2.62	0.44	2.76	0.48
B_1-6	12.70	24.90	3.03	12.80	2.38	0.48	2.82	0.53	2.53	0.50	1.44	0.23	1.49	0.26
B_1-7	4.61	9.30	1.25	5.21	2.01	0.57	4.58	1.34	9.26	2.01	6.15	1.00	5.52	0.96
B_1-F	72.60	167.00	21.80	88.20	15.40	2.49	10.50	1.68	7.97	1.66	5.18	1.00	6.54	1.06
B_2-R	48.80	92.60	9.11	32.00	5.35	0.97	4.80	1.01	6.59	1.29	3.96	0.72	4.48	0.71
B_2-1	41.90	94.40	11.40	44.40	7.63	1.60	6.37	0.93	4.62	0.85	2.55	0.48	2.54	0.42
B_2-2	3.17	6.09	0.86	3.93	1.09	0.32	1.85	0.42	2.54	0.47	1.40	0.22	1.39	0.24
B_2-3	21.50	51.50	6.63	25.30	5.28	1.02	3.90	0.67	3.38	0.70	2.25	0.42	2.44	0.41
B_2-4	71.00	114.00	12.40	48.00	7.03	1.61	5.30	0.80	3.64	0.53	1.51	0.21	1.27	0.21
B_2-5	3.62	7.85	1.12	5.62	1.88	0.70	3.05	0.77	4.46	0.90	2.65	0.43	2.14	0.33
B_2-F	50.40	96.90	10.70	34.50	7.15	2.47	9.07	1.83	10.90	1.90	5.63	0.87	5.36	0.78
B_3-R	98.20	178.00	24.10	97.50	15.70	3.31	11.10	2.11	10.30	2.75	7.26	1.01	6.53	1.02
B_3-1	7.59	17.50	1.41	5.57	1.02	0.26	0.96	0.19	1.12	0.25	0.69	0.11	0.81	0.11
B_3-2	11.80	21.50	2.39	9.47	1.97	0.34	1.88	0.34	1.62	0.39	0.99	0.19	1.24	0.16
B_3-3	17.40	33.10	3.69	13.90	3.66	0.58	3.08	0.60	3.60	0.83	2.03	0.36	2.62	0.40
B_3-4P	32.40	61.90	7.17	26.80	5.81	0.47	4.79	1.13	7.52	1.85	5.71	1.16	8.32	1.16
B_3-5	13.90	27.30	3.60	14.80	4.30	0.93	3.77	0.69	4.40	0.93	2.47	0.39	2.34	0.34
B_3-6	21.60	37.60	4.92	21.70	6.05	1.51	5.72	1.12	8.18	2.00	4.85	0.71	5.13	0.71
B_3-7	50.90	106.00	15.70	58.70	12.30	3.04	8.91	1.23	5.05	0.83	2.47	0.32	2.16	0.33

3.2 Analytical methods

The bulk samples were air-dried, crushed, ground to less than 200-mesh and dried for 2 h in a drying oven at 105°C~110°C. The samples were then preprocessed by low-temperature airproof acid digestion, whose detailed procedure is described hereafter. An accurately weighed sample of 0.0500 g was mixed with 1 ml of HF, 3 ml of HNO_3 and 1 ml of $HClO_4$ in a dedicated 25 ml digestion vessel. After the cap assembles were sealed, the vessel was put into a low-temperature electric warming plate for heating at 125°C for 24 h. Finally, the residue was dissolved with 1% HNO_3 and then transferred to a 50 ml volumetric flask. The prepared samples were then determined for their REE compositions using the inductively coupled-plasma mass spectrometry (ICP-MS) (Finnigan MAT), with the relative analysis error of ±5%, according to the "GB/T 14506.30–2010". The REEs testing was performed at the Analytical Laboratory of Beijing Research Institute of Uranium Geology. The final results were reported as the μg/g in coal with a dry basis for each sample.

4 Results

The contents of REEs and other trace elements in the C_1 coal obtained by ICP-MS analysis are presented in Tables 2, 3. The total REE content (∑REE) in C_1 coals (excluding roof, floor and Tonstein) varies from 23.99 μg/g to 267.94 μg/g, averaged 122.69 μg/g, which is slightly lower than that of average Chinese coal with 135.89 μg/g (Dai et al., 2012). Compared with the Late Permian coal in the adjacent area, the average ∑REE in C_1 coal is slightly lower than that of Yueliangtian coals from Panxian county, western Guizhou (136 μg/g, marine and continental transitional environment, cited from Wang et al., 2017), but higher than that of continental coals from Shizong county and Fuyuan county in eastern Yunnan (101 μg/g and 105.9 μg/g, respectively, cited from Wang et al., 2017 and Wang et al., 2012). The ∑REE of the roof and floor strata ranges from 212.39 μg/g to 458.89 μg/g, averaged 326.01 μg/g, which is 2.65 times of that of coal, indicating that the total amount of REEs in mudstone is significantly higher than that of coal. However, there is not significant vertical variation of REE contents among benches of individual coal seam, as seen from Figure 3.

TABLE 3 The REE and elements data of the late permian coal seam samples from the Yantang Mine, Xuanwei, Yunnan.

Sample No.	∑REE (μg/g)	HREE (μg/g)	LREE (μg/g)	L/H	$(La/Yb)_N$	δEu	δCe	Ce_{anom}	Al/Ti
B_1-R	317.22	34.96	282.26	8.07	7.27	0.84	0.80	−0.067	6.05
B_1-1	115.59	12.16	103.43	8.51	6.82	0.80	0.86	−0.050	15.61
B_1-2	151.48	15.00	136.48	9.10	9.00	0.59	0.87	−0.015	25.95
B_1-3P	308.41	54.60	253.81	4.65	3.33	0.56	0.86	−0.037	42.62
B_1-4	218.97	39.18	179.79	4.59	3.77	0.55	0.89	−0.006	41.39
B_1-5	159.78	16.52	143.27	8.67	7.16	0.57	0.85	−0.036	15.04
B_1-6	66.09	9.80	56.29	5.75	5.06	0.63	0.84	−0.048	16.61
B_1-7	53.77	30.82	22.95	0.74	0.50	0.64	0.81	−0.046	18.22
B_1-F	403.08	35.59	367.49	10.33	6.59	0.67	0.88	0.003	38.88
B_2-R	212.39	23.56	188.83	8.02	6.47	0.65	0.92	−0.030	24.47
B_2-1	220.10	18.77	201.33	10.73	9.79	0.78	0.90	0.008	27.30
B_2-2	23.99	8.53	15.46	1.81	1.35	0.76	0.77	−0.077	31.33
B_2-3	125.39	14.16	111.23	7.86	5.23	0.77	0.90	0.024	9.45
B_2-4	267.52	13.48	254.04	18.85	33.19	0.90	0.80	−0.104	15.17
B_2-5	35.52	14.73	20.79	1.41	1.00	1.00	0.81	−0.050	20.45
B_2-F	238.46	42.08	416.81	9.91	8.93	1.05	0.87	−0.027	7.82
B_3-R	458.89	4.23	33.35	7.88	5.57	0.86	0.76	−0.081	8.53
B_3-1	37.58	6.81	47.47	6.97	5.65	0.88	1.12	0.047	11.25
B_3-2	54.28	13.53	72.33	5.35	3.94	0.61	0.84	−0.061	18.73
B_3-3	85.85	31.64	134.55	4.25	2.31	0.59	0.86	−0.042	23.68
B_3-4P	166.19	15.33	64.83	4.23	3.53	0.30	0.85	−0.043	62.95
B_3-5	80.16	28.42	93.38	3.29	2.50	0.79	0.80	−0.052	18.67
B_3-6	121.80	21.30	246.64	11.58	13.99	0.88	0.76	−0.099	13.19
B_3-7	267.94	12.16	103.43	8.51	6.82	0.99	0.78	−0.035	5.14

Chondritic values by Herrmann are used for normalization with the modification of REEs (Hao et al., 2004); ∑REE=LREE+HREE; LREE=La+Ce+Pr+Nd+Sm+Eu; HREE=Gd+Tb+Dy+Ho+Er+Tm+Yb+Lu; L/H=LREE/HREE; $(La/Yb)_N = La_N/Yb_N$; $\delta Eu = Eu_N/(Sm_N \times Gd_N)^{1/2}$; $\delta Ce = Ce_N/(La_N \times Pr_N)^{1/2}$;N stands for chondrite normalization; Data of Ti and Al are cited from Shao et al., 2015.

The REEs contents of chondrites were taken from Herrmann (Hao et al., 2004) and the chondrite-normalized REE distribution patterns of all samples from the seam C_1 are showed in Figure 3. All of the curves show a certain slope and are tilted to the right. The curves of Light REE (LREE) are slightly sloping compared with Heavy REE (HREE). The samples from seam B_1 and B_3 show a similar distribution trend respectively, while the curves of samples from seam B_2 are haphazard. The $(La/Yb)_N$ ratios of all samples change from 0.50 to 33.19, with an average value of 6.73, indicating that LREE were significantly enriched relative to HREE. This is consistent with all other studies which reveal the predominance of the LREE relative to HREE.

Most samples of the C_1 coal are depleted in Eu at various degrees, with δEu values ranging from 0.55 to 1.00 for an average of 0.74, and with a peak negative value (0.30) appearing in Tonstein B_3-4. The δCe value of C_1 coals show slightly negative or free anomalies, ranging from 0.76 to 1.12, averaged 0.85.

The REE patterns may be subsequently altered to a variable extent by post-depositional, diagenetic exchange or surface weathering (Zeng et al., 2001; Blake et al., 2017). As a special organic sedimentary rock, coal may also be affected by the above-mentioned factors during the coal-forming process, which could affect REEs fractionation and enrichment. For instance, δCe value easily changes due to diagenesis, which then leads to a significantly positive correlation between δCe and δEu, a significantly negative correlation between δCe and $(Dy/Sm)_N$, and a significantly positive correlation between δCe and ∑REE (Shields et al., 2001; Zeng et al., 2011; Qu et al., 2018). To confirm the influence of diagenesis on samples from seam C_1, the above three correlation coefficients are calculated as -0.10, 0.15 and 0.18, respectively (Figure 4). The correlation values are not significant, showing that diagenesis has very little influence on the Ce anomaly in the C_1 coal. In consideration of this result, the Ce anomaly is regarded to reflect the characteristics of the terrestrial environment during sedimentary period as it represents the information of the original samples.

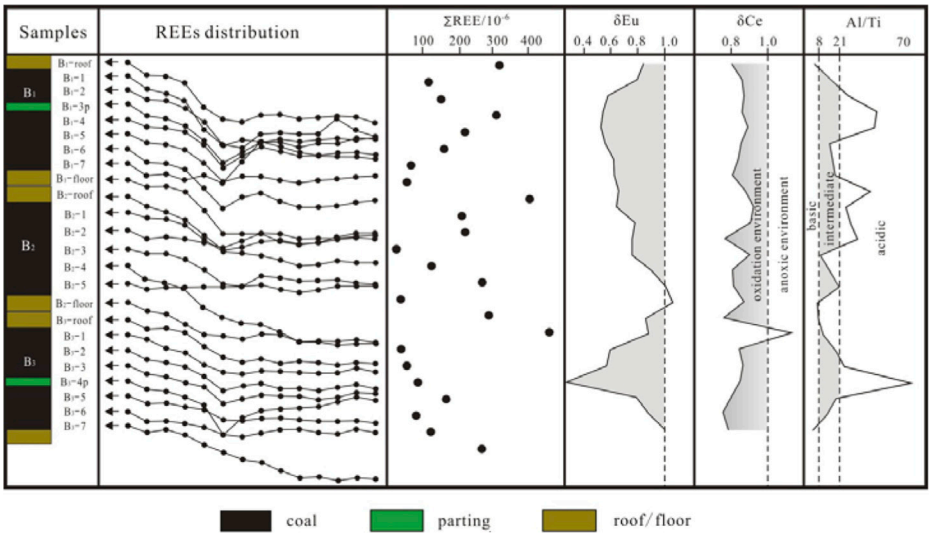

FIGURE 3
Stratigraphic distribution of patterns of ∑REE, δEu, δCe and Zr/Hf in all coal samples from Yantang Mine, Xuanwei, Yunnan.

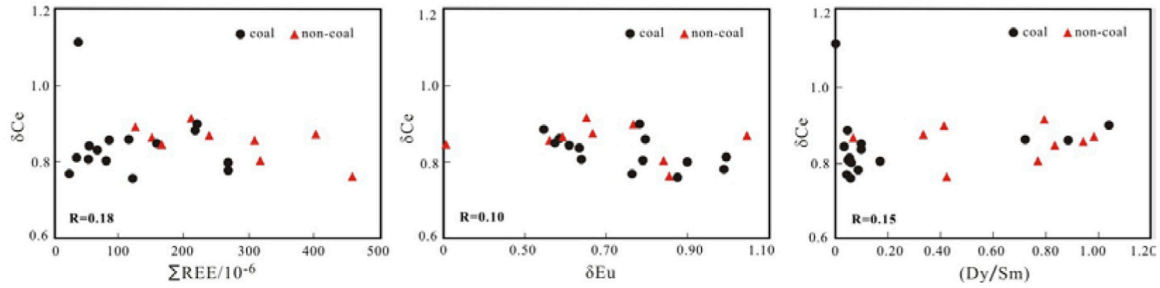

FIGURE 4
δCe correlate with δEu, $(Dy/Sm)_N$ and ∑REE in the C_1 coal of Yantang Mine, Xuanwei, Yunnan.

5 Discussion

5.1 Sedimentary environment

Ce anomaly is an effective redox indicator, which can be used to analyze sedimentary environment and paleo-water medium conditions. The δCe greater than 1 indicates a reducing condition, while that less than 1 reflects a more oxidizing condition (Qu et al., 2018). In general, the negative Ce anomaly indicates the marine sedimentary environment, while the mafic basalt has slightly positive or free Ce anomaly (Zhao et al., 2019; Wang et al., 2020). The δCe of samples from the seam C_1 are mostly between 0.76 and 0.92, averaged 0.84, indicating a slightly negative Ce anomaly (Table 3 and Figure 3), which is significantly different from the REE characteristics of seawater (Qu et al., 2018; Huang et al., 2019). Therefore, the influence of sea water can be excluded. The above discussion of δCe in samples from seam C_1 suggested that the coal-forming peatland was affected by the input of basic basalt clastic materials from the Khangdian Oldland, and the coalforming peatland was in weak oxidation environment.

In addition, Ce_{anom} is also widely used in the identification of paleoredox conditions. The Ce_{anom} is greater than 0 indicates water hypoxia, while that less than 0 reflects oxidized water (Tian et al., 2018). Most Ce_{anom} of samples from seam C_1 are less than 0 (Table 2), indicating the weak oxidation environment of coal-forming peatland. Only a few samples in seam B_2 have Ce_{anom} greater than 0, indicating that peatland oxidation and reduction environments alternate during coalforming, suggesting a turbulent coal-forming environment.

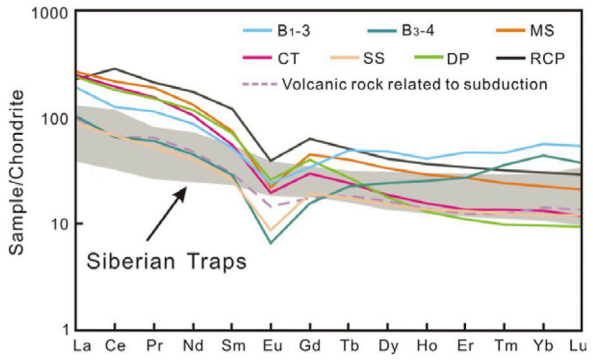

FIGURE 5
Chondrite-normalized REE patterns of the tonsteins in the C_1 coal, PTB volcanic ashes and subduction-related rock.

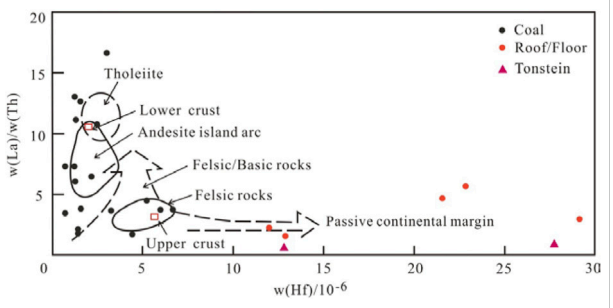

FIGURE 6
w(La)/*w*(Th)—*w*(Hf) discrimination diagram for provenance attribute Data of Zr and Hf are cited from Shao et al. (2015).

5.2 The character of volcanic ash

Eu anomaly is inherited from the source rock, and as such Eu is generally recognized as an indicator of the nature of provenances. Basalt shows mostly no negative Eu anomaly, while granite and other acidic rocks present obvious negative Eu anomaly (Chen et al., 1990; Wang et al., 2019). Since the main provenance area of the coal-bearing basin in the study area is basalt (and its weathering and alteration products) originating from Khangdian Oldland, there should be no Eu anomaly in the C_1 coal samples. However, most coal bench samples of the C_1 seam are depleted in Eu at various degrees (Figure 3 and Table 2), except those at the roofs and floors and their vicinity. According to the sedimentary sequence of the C_1 coal, the bottom coal of seam B_3 that was first deposited has no Eu anomaly, and then the degree of negative Eu anomaly increases gradually upward, and reaches the maximum value of the whole coal seam rapidly at Tonstein B_3-4 (δEu is 0.30), and then decreases rapidly upward. There was no Eu anomaly in the floor and bottom coal of the sub-seam B_2 which deposited followed by the sub-seam B_1, and the degree of negative Eu anomaly increased slowly from the bottom of sub-seam B_2 upward to sub-seam B_1 (B_1-4) and Tonstein (B_1-3), reaching the maximum Eu negative anomaly, and then the Eu negative anomaly decreased rapidly. The Eu negative anomaly degree of Tonstein B_1-3 is significantly lower than that of B_3-4, which may be caused by the input of acidic volcanic materials, and acidic volcanic activities are more intense during the B_3 coal-forming period.

The Al in normal igneous rocks resides mostly in feldspars and the Ti in mafic minerals. Therefore, the Al/Ti ratio is an important parameter to determine the parent rock composition. Generally, basic rock with a Al/Ti ratio of 3–8 and intermediate rock with a Al/Ti ratio of 8–21, 21–70 indicate acidic rock (Hayashi et al., 1997). The Al/Ti ratio of Tonstein B_1-3 and B_3-4 is 42.62 and 62.95, respectively, whereas that of most coals is between 9.45 and 41.39 (Table 3). Integration of δEu and Al/Ti ratios suggest that there were twice significantly acidic volcanic activities during coal-forming (Figure 7A).

Tonstein is the preserved "relic" of volcanic activity, the δEu with 0.56 and 0.30 of Tonstein B_1-3 and B_3-4 are very close to that of five typical PTB ash beds in South China (He et al., 2014; Tan et al., 2019), so it is inferred that the two volcanic activities are the same provenance with those indicated by the PTB volcanic ash layer in South China. Furthermore, the similar shaped curves and negative Eu anomaly indicate that the Tonsteins and ash beds have the same REE origin from volcanic rocks related to plate subduction (Siberian Traps) (Widiatama et al., 2021) (Figure 5).

5.3 Source and tectonic background of the C_1 coal

REEs have special geochemical characteristics, and are stable during weathering, erosion, transportation, deposition and early diagenesis. Therefore, the REEs have been used to infer the material source of sediments (Bai et al., 2015; Tian et al., 2018; Qu et al., 2018). The different chondrite-normalized patterns of sub-seam B_1, B_2 and B_3 (Figure 3) show different coal-forming process. With few exceptions, the distribution curves of REEs in the first deposited sub-seam B_3 are most similar, indicating the stable and single provenance. The distribution curves and abundance of REEs in samples from the sub-seam B_2 have more variability than sub-seam B_3. In addition, Ce_{anom} of samples reflected that the oxidation and reduction environment appeared alternately during coal-forming of sub-seam B_2. All of the above results indicate that the sedimentary environment of peat swamp was relatively turbulent and the provenance was unstable during this period. The distribution curves of REEs in the latest sub-seam B_1 are slightly different. Besides, the abundance of ∑REE in top coal suddenly decreases, inferred that the input of terrigenous substances replaces the paleoplant, and finally leads to the termination of coal-forming process.

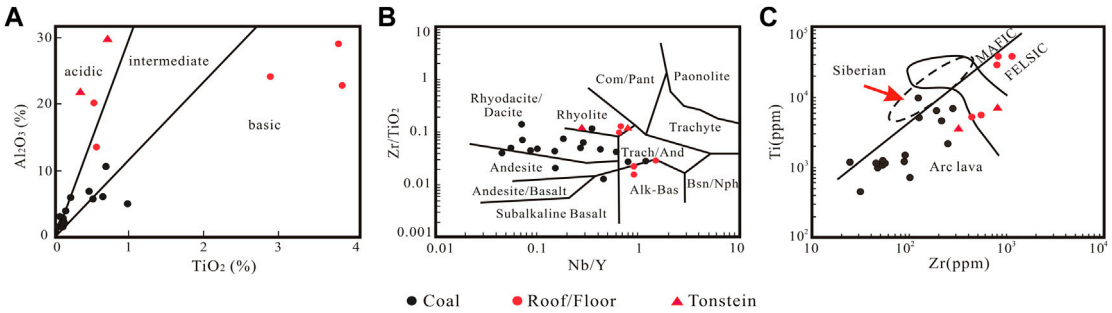

FIGURE 7
(A) Zr versus Ti diagram (modified from He et al., 2014), **(B)** plots of mass fractions of Al_2O_3 *versus* TiO_2, and **(C)** Zr/TiO_2 versus Nb/Y diagram (modified from He et al., 2014).

Diagrams of *w*(La)/*w*(Th)—*w*(Hf) is commonly used to discriminate the source rocks and tectonic setting (Bai et al., 2015; Qu et al., 2018). The result shows that coals from the seam C_1 are from multiple sources, such as tholeiite, andesite island arc, felsic and basic rocks (Figure 6). Tonsteins, seam roofs and floors are plotted mainly into the felsic and basic rocks area (Figure 6). All samples from the seam C_1 are deposited in the passive continental margin.

Tonsteins in the seam C_1 classify as acidic rock on the Al_2O_3 *versus* TiO_2 and diagram of Nb/Y—Zr/TiO_2 (Figures 7A,B), and Tonsteins originate from felsic magmatic arc.

Integration of dispersion of coal samples plotted in above diagrams and variation of distribution curves of REEs, it can be inferred that the provenance of C_1 coal is complex and influenced by the input of basalt and acidic volcanic ash during coal-forming process (Figures 3, 6, 7). Concretely, the roofs and floors originated from the basalt clastic materials of the KhangDian Oldland, while the Tonstein layer is derived from the acidic synsedimentary volcanic ash. Based on the dual influence of volcanism and basic basalt clastic material, the source rocks of the coal seam C_1 show basic, intermediate and acidic (Figure 7A).

5.4 The relationship between coal formation and volcanic activity

During the Permian-Triassic, the Paleo-Tethys along a subduction zone between the South China and Indochina cratons closed gradually, and Indochina Plate moved rapidly northward and collided with other plates, consequently felsic volcanic activities were extraordinarily active(Cawood, 2005; Wang et al., 2019; Zhao et al., 2019) (Figure 8A). During one eruption, dust nanoparticles can travel thousands of kilometers through the stratosphere and affect all areas of the Earth for years (Ermolin et al., 2018). The volcanic ash falling to South China was altered in different sedimentary environments to form kaolinite, illite or illite/smectite, such as Tonsteins interbedded in C_1 coal from Xuanwei area and five typical marine PTB sections in South China (Figures 8B,C) (He et al., 2014; Wang et al., 2018). Multiple volcanic claystone beds are widely developed in South China, which become more frequent and thicker towards southwest margin of Yangtze, indicating that the source of PTB tuff and volcanic claystone is in the southwest margin of the Yangtze Plate (Sun et al., 2013; Wang et al., 2022). Recently, previous studies on the source of PTB volcanic ash in South China have shown that, the PTB volcanism occurred near southwest South China and their adjacent convergent continental margin due to the closure of Paleo-Tethys. Furthermore, volcanic ash derived from subduction-zone arc between South China and Indochina cratons, which is not the trigger of PTB mass extinction due to limited eruption (Isozaki et al., 2007; Zhao et al., 2013; He et al., 2014; Wang et al., 2018; Wang et al., 2019; Zhao et al., 2019; Hou et al., 2020).

The age of Tonstein (252.0 ±2.3 Ma, Wang et al., 2018) of the sub-seam B_1 overlaps with age of granite (235–252 Ma, Ma et al., 2019) as evidence of subduction-zone, and Xuanwei area is immediately adjacent to the continental magmatic arc of the southwest margin of the South China at the End-Permian (Wang et al., 2018). By comparing REE patterns of two Tonsteins, five typical PTB volcanic ash layers, volcanic rocks related to subduction and Siberian traps (Figure 5) (He et al., 2014; Liu et al., 2015), it is found that the distribution curves of the first three are very similar, except the last one, mainly due to the absence of negative Eu anomaly. In addition, the REE patterns of Tonsteins are slightly different from those of PTB volcanic ash layers, such as little fractionation of LREE and HREE and flatter distribution curve, which may be caused by the volcanic ash falling in different sedimentary environments. Tonsteins were deposited in continental fluvial sedimentary environment, and the input of terrigenous materials tends to flatten the distribution curves of REE, which is different from the marine PTB volcanic

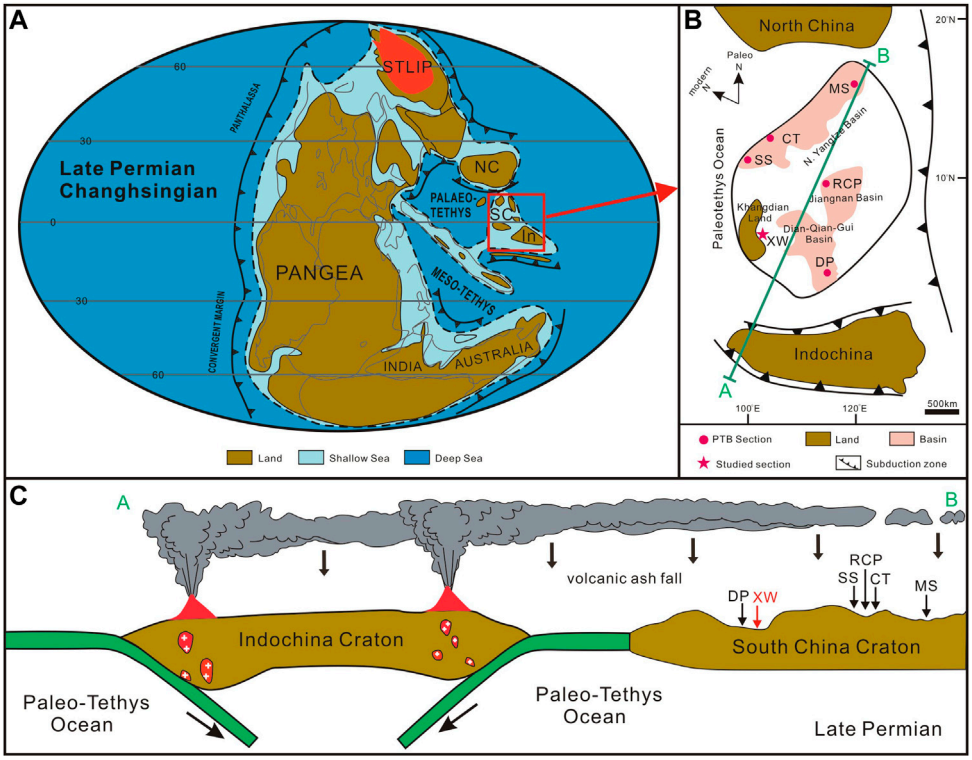

FIGURE 8
(A) Global paleogeography at late permian (Changhsingian) (modified from Metcalfe, 2013; Wang et al., 2019); **(B)** Potential volcanic ash source areas and inferred direction of ash transport (A→B) in South China and Indochina area during late permian (modified from Wang et al., et al., 2018; Zhao et al., 2019); **(C)** Composite cross-section of Late Permian South China and Indochina Craton, showing subduction of the Paleo-Tethys Plate beneath the Indochina Craton margin (modified from Wang et al., 2018; Zhao et al., 2019). Abbreviations in A: STLIP-Siberian Traps Large Province; NC-North China; SC-South China; In-Indochina Craton; B: DP-Dongpan, XW-Xuanwei, SS-Shangsi, RCP-Rencunping, CT-Chaotian, MS-Meishan.

ashes (Liu et al., 2018). The diagrams of Al_2O_3-TiO_2, Nb/Y-Zr/TiO_2 and Zr-Ti (Figure 7) also confirmed that the two layers of Tonstein derived from volcanic magmatic arc and were acidic, which was different from the basic SLIP (Kamo et al., 2003). Therefore, it was inferred that Tonsteins in the C_1 coal were from felsic volcanism of the End-Permian, rather than SLIP.

Significantly, the bottommost coal sample B_3-7, which has been plotted in the SLIP area (Figure 7C), and its δEu of 0.99, Al/Ti of 5.14, REE pattern curve and diagram of *w*(La)/*w*(Th)-*w*(Hf) and Zr-Ti, indicating that it has been affected by basic basalts. It is further confirmed that C_1 coal was influenced by SLIP in its early stage. Compared with Indochina craton, SLIP and eastern Yunnan Province are more far apart. However, the SLIP is known as the largest continental volcanic event since Phanerozoic, and volcanic ash nanoparticles can transport to worldwide. With the overlap between constraint on SLIP eruption and C_1 coal forming, therefore it can be inferred that the C_1 coal was affected by SLIP in the early stage of coal forming.

6 Conclusion

The C_1 coal from Xuanwei County, Yunnan Province contains two layers of Tonstein. REEs, several major and trace elements data indicate the following:

(1) The total REE content of the C_1 coal ranges from 23.99 to 267.94 μg/g, averaged 122.69 μg/g. C_1 coal samples are enriched in LREE relative to HREE and show significant fractionation between LREE and HREE. Most samples including coals, Tonsteins, roofs and floors present varying degrees of negative Eu anomaly, especially two Tonsteins in sub-seam B_1 and B_3 with the significant negative Eu anomalies. Most samples of the seam C_1 are slightly depleted in Ce.
(2) The C_1 coal-forming peatland was affected by the input of basic basalt clastic materials from Khangdian Oldland and acidic volcanic ash. The C_1 coal was deposited in a weak oxidation environment, and experienced turbulent

environment during the middle and later stage of coal-forming period.

(3) The geochemical characteristics of Tonsteins in the C_1 coal are similar to those of the marine PTB volcanic ash layers in South China, which are both derived from the felsic volcanism caused by the closure of the Paleo-Tethys at the southwestern margin of the South China. Furthermore, the C_1 coal was also affected by the eruption of SLIP in the early stage.

Data availability statement

The original contributions presented in the study are included in the article/supplementary material, further inquiries can be directed to the corresponding author.

Author contributions

JW searched the literature; JW and LS analyzed the data and wrote the paper; ZY and XW collected samples and performed the experiments.

Funding

This work is supported by the National Natural Science Foundation of China (No. 41602123 and 41572090), and the Fundamental Research Funds for the Universities of Henan Province (No. NSFRF220401).

Conflict of interest

The authors declare that the research was conducted in the absence of any commercial or financial relationships that could be construed as a potential conflict of interest.

Publisher's note

All claims expressed in this article are solely those of the authors and do not necessarily represent those of their affiliated organizations, or those of the publisher, the editors and the reviewers. Any product that may be evaluated in this article, or claim that may be made by its manufacturer, is not guaranteed or endorsed by the publisher.

References

Arbuzov, S. I., Maslov, S. G., Finkelman, R. B., Mezhibor, A. M., Ilenok, S. S., Blokhin, M. G., et al. (2018), Modes of occurrence of rare Earth elements in peat from Western Siberia Rare Earth and major element geochemistry of Eocene fine-grained sediments in oil shale- and coal-bearing layers of the Meihe Basin, Northeast China. *J. Asian Earth Sci. of Geochemical Exploration* 184, 4089–48101 97

Blake, J. M., Peters, S. C., and Johannesson, K. H. (2017). Application of REE geochemical signatures for mesozoic sedimentprovenance to the gettysburg basin, Pennsylvania. *Sediment. Geol.* 349, 103–111. doi:10.1016/j.sedgeo.2016.12.009

Cawood, P. A. (2005). Terra australis orogen: Rodinia breakup and development of the pacific and iapetus margins of gondwana during the neoproterozoic and paleozoic. *Earth. Sci. Rev.* 69, 249–279. doi:10.1016/j.earscirev.2004.09.001

Chen, D. Q., and Chen, G. (1990). *Practical geochemistry of rare earth elements*. Beijing: Metallurgical Industry Press, 228–230. (in Chinese).

Dai, S. F., Ren, D. Y., Chou, C. L., Finkelman, R. B., Seredin, V. V., and Zhou, Y. P. (2012). Geochemistry of trace elements in Chinese coals: A review of abundances, genetic types, impacts on human health, and industrial utilization. *Int. J. Coal Geol.* 94 (3), 3–21. doi:10.1016/j.coal.2011.02.003

Ermolin, M. S., Fedotov, P. S., Malik, N. A., and Karandashev, V. K. (2018). Nanoparticles of volcanic ash as a carrier for toxic elements on the global scale. *Chemosphere* 200, 16–22. doi:10.1016/j.chemosphere.2018.02.089

Guo, B. Q., Gao, D., Guo, H. L., Liu, J. G., Wang, J. H., and Shi, Y. (2022). Geochemistry of the Permian–Triassic boundary strata in the southwest margin of the North China Craton: Provenance and tectonic implications. *Geol. J.*,23 1–14. doi:10.1002/gj.4558

Hao, L. B., and Qi, C. M. (2004). *Principles of geochemistry*, 2. Beijing: Geological Press, 54–55. (in Chinese)., pp.

Hayashi, K. I., Fujisawa, H., Holland, H. D., and Ohmoto, H. (1997). Geochemistry of ~1.9 Ga sedimentary rocks from northeastern Labrador, Canada. *Geochimica Cosmochimica Acta* 61 (19), 4115–4137. doi:10.1016/s0016-7037(97)00214-7

He, B., Zhong, Y. T., Xu, Y. G., and Li, H. X. (2014). Triggers of permo-triassic boundary mass extinction in South China: The siberian traps or paleo-tethys ignimbrite flare-up? *Lithos* 204, 258–267. doi:10.1016/j.lithos.2014.05.011

Hedin, B. C., Capo, R., Stewart, B. W., Hedin, R. S., Lopano, C. L., and Stuckman, M. Y. (2019). The evaluation of critical rare Earth element (REE) enriched treatment solids from coal mine drainage passive treatment systems. *Int. J. Coal Geol.* 208, 54–64. doi:10.1016/j.coal.2019.04.007

Hou, H. H., Shao, L. Y., Tang, Y., Li, Y. N., Liang, G. D., Xin, Y. L., et al. (2020). Coal seam correlation in terrestrial basins by sequence stratigraphy and its implications for palaeoclimate and palaeoenvironment evolution. *J. Earth Sci.*, 1–24.

Huang, Q. H., Bai, X. F., Wang, H., Cheng, H. G., and Zhu, Z. Y. (2019). Geochemical characteristics and geological significance of trace elements and rare Earth elements in carbonate rocks at Middle-Upper Permian boundary in Linxi area, Inner Mongolia. *Glob. Geol.* 38 (3), 611–622.

Isozaki, Y., Shimizu, N., Yao, J. X., Ji, Z. S., and Matsuda, T. (2007). End-Permian extinction and volcanism-induced environmental stress: The Permian-Triassic boundary interval of lower-slope facies at Chaotian, South China. *Palaeogeogr. Palaeoclimatol. Palaeoecol.* 252, 218–238. doi:10.1016/j.palaeo.2006.11.051

Kamo, S. L., Czamanske, G. K., Amelin, Y., Fedorenko, V. A., Davis, D. W., and Trofimov, V. R. (2003). Rapid eruption of Siberian flood-volcanic rocks and evidence for coincidence with the Permian-Triassic boundary and mass extinction at 251 Ma. *Earth Planet. Sci. Lett.* 214, 75–91. doi:10.1016/s0012-821x(03)00347-9

Liu, D. N., Zhou, A. C., and Chang, Z. G. (2015). Geochemistry characteristics of major and rare Earth elements in No.8 raw and weathered coal from Taiyuan Formation of Datong coalfield. *J. China Coal Soc.* 40 (2), 422–430. (in Chines, with English abstract).

Liu, Q. Q., Chi, Q. H., Wang, X. Q., Zhou, J., Liu, H. L., Liu, D. S., et al. (2018). Distribution and influencing factors of rare Earth elements in carbonate rocks along three continental-scale transects in eastern China. *Earth Sci. Front.* 25 (4), 99–115. (in Chines, with English abstract).

Ma, X. H., Chen, C. J., Zhao, J. X., Qiao, S. L., and Zhou, Z. H. (2019). Late permian intermediate and felsic intrusions in the eastern central asian orogenic belt: Final-stage magmatic record of paleo-asian oceanic subduction? *Lithos* 326-327, 265–278. doi:10.1016/j.lithos.2018.12.022

Metcalfe, I. (2013). Gondwana dispersion and Asian accretion: Tectonic and palaeogeographic evolution of eastern Tethys. *J. Asian Earth Sci.* 66, 1–33. doi:10.1016/j.jseaes.2012.12.020

Munir, M. A. M., Liu, G. J., Yousaf, B., Ali, M. U., Abbas, Q., and Ullah, H. (2018). Enrichment of Bi-Be-Mo-Cd-Pb-Nb-Ga, REEs and Y in the permian coals of the huainan coalfield, anhui, China. *Ore Geol. Rev.* 95, 431–455. doi:10.1016/j.oregeorev.2018.02.037

Qu, X. R., Li, J., Sun, C. R., Zhang, Q. H., Tang, S. H., and Wei, J. G. (2018). Geochemistry characteristics of rare Earth elements in the late Paleozoic black shale from eastern Ordos Basin. *J. China Coal Soc.* 43 (4), 1083–1093. (in Chinese, with English abstract).

Ren, D. Y., Zhao, F. H., Dai, S. F., Zhang, J. Y., and Luo, K. L. (2006). *Trace element geochemistry of coal*. Beijing: Science Press, 321–334. (in Chinese).

Shao, L. Y., Gao, C. X., Zhang, C., Wang, H., Guo, L. J., and Gao, C. H. (2013). Sequence-palaeogeography and coal accumulation of late permian in southwestern China [J]. *Acta sedimentol. sin.* 31 (5), 856–866. (in Chinese, with English abstract).

Shao, L. Y., Wang, J., Hou, H. H., Zhang, M. Q., Wang, H., Spiro, B., et al. (2015). Geochemistry of the C_1 coal of latest permian during mass extinction in Xuanwei, yunnan. *Acta Geol. sin.* 89 (1), 163–179. (in Chinese, with English abstract).

Shields, G., and Stille, P. (2001). Diagenetic constraints on the use of cerium anomalies as palaeoseawater redox proxies: An isotopic and REE study of Cambrian phosphorites. *Chem. Geol.* 175 (1-2), 29–48. doi:10.1016/s0009-2541(00)00362-4

Sun, Y. D. (2013). *Coupling climatic and biodiversity changes with volcanisms during the Palaeozoic-Mesozoic upheavals in South China*. Wuhan: China University of Geosciences PhD thesis. (in Chinese with English abstract).

Tan, C., Yuan, X. J., Yu, B. S., Liu, C., Li, W., and Cui, J. W. (2019). Geochemical characteristics and paleoclimatic implications of the upper permian and middle-lower triassic strata in southern ordos basin. *GEOSCIENCE* 33 (3), 615–628. (in Chinese with English abstract).

Tian, X. L., Luo, K. L., Wang, S. B., and Ni, R. X. (2014). Geochemical characteristics of trace elements and rare Earth elements during the Cryogenian-Ediacaran transition in Yangtze Gorges area. *J. Palaeogeogr.* 16 (4), 483–502. (in Chinese, with English abstract).

Ulrich, M., Cathelineau, M., Munoz, M., Boiron, M. C., Teitler, Y., and Karpoff, A. M. (2019). The relative distribution of critical (Sc, REE) and transition metals (Ni, Co, Cr, Mn, V) in some Ni-laterite deposits of New Caledonia. *J. Geochem. Explor.* 197, 93–113. doi:10.1016/j.gexplo.2018.11.017

Wang, H., Shao, L. Y., Hao, L. M., Zhang, P. F., Glasspool, I. J., Wheeley, J. R., et al. (2011). Sedimentology and sequence stratigraphy of the Lopingian (Late Permian) coal measures in southwestern China. *Int. J. Coal Geol.* 85, 168–183. doi:10.1016/j.coal.2010.11.003

Wang, H., Shao, L. Y., Newton, R. J., Bottrell, S. H., Wignall, P. B., and Large, D. J. (2012). Records of terrestrial sulfur deposition from the latest Permian coals in SW China. *Chem. Geol.* 292-293, 18–24. doi:10.1016/j.chemgeo.2011.11.005

Wang, J., Shao, L. Y., Wang, H., Spiro, B., and Large, D. (2018). SHRIMP zircon U-Pb ages from coal beds across the Permian-Triassic boundary, eastern Yunnan, southwestern China. *J. Palaeogeogr.* 7 (2), 117–129. doi:10.1016/j.jop.2018.01.002

Wang, P. P. (2017). *Enrichment and differentiation mechanism of minerals and trace elements in the Late Permian coals from eastern Yunnan and western Guizhou Province*. Beijing: China University of Mining and Technology PhD thesis. (in Chinese, with English abstract).

Wang, Q., and Yang, R. D. (2008). Tracing study on REEs of coal measure in late permian in bijie city, Guizhou province, China. *J. Chin. rare earth Soc.* 26 (1), 102–107. (in Chinese, with English abstract).

Wang, T., Zhu, X. M., Dong, Y. L., Chen, H. H., Su, B., Liu, Y., et al. (2020). Trace elements as paleo sedimentary environment indicators: A case study of the paleogene anjihaihe formation in the northwestern junggar basin. *Acta Geol. Sin.* 94 (12), 3830–3851. (in Chinese with English abstract).

Wang, X. B., Dai, S. F., Chou, C. L., Zhang, M. Q., Wang, J. M., Song, X. L., et al. (2012). Mineralogy and geochemistry of late permian coals from the taoshuping mine, yunnan province, China: Evidences for the sources of minerals. *Int. J. Coal Geol.* 96-97, 49–59. doi:10.1016/j.coal.2012.03.004

Wang, X. D., Cawood, P. A., Zhao, L. S., Chen, Z. Q., Lyu, Z. Y., and Ma, B. (2019). Convergent continental margin volcanic source for ash beds at the Permian-Triassic boundary, South China: Constraints from trace elements and Hfisotopes. *Palaeogeogr. Palaeoclimatol. Palaeoecol.* 519, 154–165. doi:10.1016/j.palaeo.2018.02.011

Wang, Y., Cao, J., Zhang, B. L., Liao, Z. W., Zhang, B., Liu, J. C., et al. (2022). Genesis of the wangpo bed in the sichuan basin: Formation by eruptions of the emeishan large igneous province. *Palaeogeogr. Palaeoclimatol. Palaeoecol.* 2022 (594), 110935. doi:10.1016/j.palaeo.2022.110935

Widiatama, A. J., Natalia, H. C., Ikhram, R., Santy, L. D., Wahyudiono, J., Wiguna, L. R. S., et al. (2021). Pedaro formation, equivalent of plover sandstone at savu island, outer banda arc. *IOP Conf. Ser. Earth Environ. Sci.* 882 (1), 012052–012044. doi:10.1088/1755-1315/851/1/012052

Wu, D., Sun, R. Y., and Liu, G. J. (2013). Characterization of REE geochemistry of the permian coals from the zhuji coal mine. *Huainan Coalf. its Geol. Implic. Acta Geol. sinica* 87 (8), 1158–1166. in Chinese, with English abstract.

Xie, Y. Y., Meng, J., and Guo, L. F. (2014). REE geochemistry of modern eolian dust deposits in Harbin city, Heilongjiang province, China: Implications for provenance. *Catena* 123, 70–78. doi:10.1016/j.catena.2014.07.008

Zeng, J. W., Xu, R., and Gong, Y. M. (2011). Hydrothermal activities and seawater acidification in the Late Devonian F-F transition: Evidence from geochemistry of rare Earth elements. *Sci. China Earth Sci.* 54, 540–549. (in Chinese, with English abstract). doi:10.1007/s11430-011-4171-8

Zhao, L. S., Chen, Z. Q., Algeo, T. J., Chen, J. B., Chen, Y. L., Tong, J. N., et al. (2013). Rare Earth element patterns in conodont albid crowns: Evidence for massive inputs of volcanic ash during the latest Permian biocrisis? *Glob. Planet. Change* 105, 135–151. doi:10.1016/j.gloplacha.2012.09.001

Zhao, T. Y., Algeo, T. J., Feng, Q. L., Zi, J. W., and Xu, G. Z. (2019). Tracing the provenance of volcanic ash in Permian-Triassic boundary strata, South China: Constraints from inherited and syn-depositional magmatic zircons. *Palaeogeogr. Palaeoclimatol. Palaeoecol.* 516, 190–202. doi:10.1016/j.palaeo.2018.12.002